Chapter 6

Design of a compact smartphone optical system for interferometric based sensing investigations

The design of a smartphone platform optical interferometric tool has been discussed. Details about the optical system developed for converting the smartphone in to a interferometric system has been illustrated and the utility of the smartphone applications for onboard fringe processing has been discussed. The usability of the developed platform has been demonstrated for monitoring of change in phase difference in an interferometric process. Using 3D printing technology, the interferometric optical set-up has been obtained which can be integrated easily with the smartphone and the usability of the new set-up has been demonstrated for measurement of small angular variations.

6.1 Introduction

Optical interferometry is considered as one of the most sensitive and widely used technique in optical metrological application because this technique is sensitive down to sub-wavelength scale [1]. It is extensively used in many diverse scientific areas that includes astronomy, fiber optics sensing, seismology, and imaging etc [2-5]. In optical metrology, interferometry is largely used for accurate measurement of various physical parameters such as surface flatness, thickness, inclination planes etc [6]. The system used to study the interferometry is called interferometer. In an optical interferometric process, two coherent light beam combine to form interference fringes in which characteristic parameters such as intensity and width of the fringes depend on the wavelength (λ), optical path difference (OPD) between the light beams and the refractive index (n) of the medium [7].

Therefore, by studying the fringe pattern, one can estimate many physical parameters such as length and refractive index etc. Almost all interferometric detection processes used in optical metrology are based on the fringe counting, intensity measurement and phase analysis [8-11]. The measurement process in an optical interferometer requires sophisticated computational facility for automatic fringe counting or phase analysis, rigorous opto-mechanical parts and detectors such as CCD or CMOS camera. These limit the portability of an interferometric system beyond a sophisticated laboratory environment which eventually limits its applicability for different in-field applications. Besides, its usability for measuring of physical parameters, optical interferometry has been demonstrated as an ultra sensitive sensing technique for many bio-chemical and environmental monitoring applications [12-14]. Thus, the need of field portable and low-cost interferometric systems could be a promising alternative for different in-field applications.

As discussed in chapter 1, due to the inclusion of high megapixel count camera and onboard image processing capabilities in smartphone, many research groups have demonstrated the usability of smartphone in spectroscopic, microscopic and colorimetric sensing applications [15]. The high megapixel count camera facilitates the development of smartphone spectrometer with resolution as low as 1 nm [16] and the smartphone based imaging platform which can even image single DNA molecule [17]. Hossain et al. has demonstrated the usability of smartphone camera in laser beam profiling [18]. Besides smartphones, the advent of rapid 3D printing technology promotes the development of sophisticated opto-mechanical components required for optics holding which can be used as a low cost alternatives over its costly commercial counterparts [19]. In this chapter, design of a smartphone based interferometric system and its usability has been demonstrated in measuring of some physical parameters in the interferometric process. At first, the camera embedded in the smartphone has been used for recording interference fringes and post processing analysis has been carried out using imageJ software in a PC. In this case, the optical set-up has been fabricated using CNC machining technology. The developed interferometric system has been used to monitor optical phase change in the interfering light beams from a microscopic glass slide by changing the incident angle through rotation. Also the developed interferometric system has been obtained through rapid 3D printing. A custom designed appli-

cation has been used to demonstrate onboard fringe processing within the phone itself. The attached compact 3D printed optical set-up has been used to measure small angular rotations.

6.2 Working principle of the designed smartphone platform interferometric system

In the present work, the interference fringes has been obtained by division of amplitude of the incident waveform from a reflection scheme. As shown in figure 6.1, a plane-parallel microscopic glass slide of thickness t has been illuminated with a monochromatic point source **S**. An observational point **P1** receive two light rays reflected from the top and bottom surface of the glass slide where the two rays interfere with each other and produce interference fringes based on their optical path difference. Due to symmetry, the interference fringes formed by this scheme is circular. As shown figure 6.1, at **P1** and its symmetric point **P2** of the plane of observation, a circular bright or dark fringe will be formed based on OPD between the two interfering beams and this would depend on the angle of incidence i. Any small change in inclination of the glass slide would cause a variation in OPD between the interfering rays. This would lead to the variation in fringe intensity pattern. The change in optical path difference between the two interfering rays is given by

$$OPD = 2nt\cos\phi \tag{6.1}$$

where, n is the refractive index of the glass slide and ϕ is the angle of refraction. Considering a phase change of π on the reflected light from the top surface of the glass slide ($n_{glass} > n_{Air}$), the condition for destructive interference can be written as

$$OPD = 2nt\cos\phi = m\lambda \tag{6.2}$$

and for constructive interference

$$OPD = 2nt\cos\phi = (m + \frac{1}{2})\lambda \tag{6.3}$$

where, λ is the wavelength of the incident light and m is the fringe order. Again,

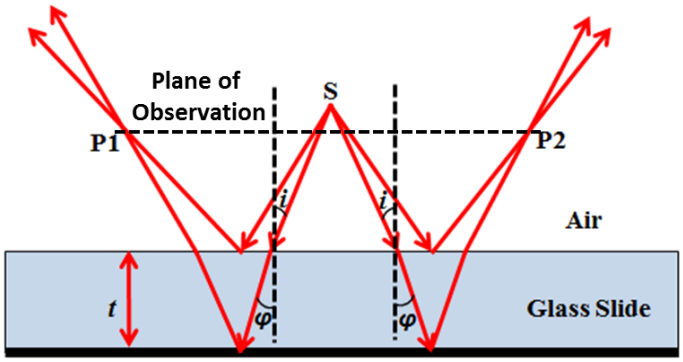

Figure 6.1: Schematic representation of the interference phenomenon which occurs as a result of back-reflection of the incident light signal from a glass plate.

law of refraction gives

$$\sin i = n \sin \phi \tag{6.4}$$

Considering small angle approximation, equation 6.4 can be written as

$$i = n\phi \tag{6.5}$$

Thus, equation 6.3 can be written as in terms of incident angle i which is given by

$$2nt\{1 - \frac{i^2}{2n^2}\} = (m + \frac{1}{2})\lambda \tag{6.6}$$

If the glass plate is rotated from an initial angle i_A to an angle i_B then the change in OPD can be written as:

$$OPD_B - OPD_A = 2nt\{(1 - \frac{{i_B}^2}{2n^2}) - (1 - \frac{{i_A}^2}{2n^2})\} = \{(m_B + \frac{1}{2}) - (m_A + \frac{1}{2})\}\lambda \tag{6.7}$$

or

$$\frac{t}{n}({i_B}^2 - {i_A}^2) = (m_B - m_A)\lambda \tag{6.8}$$

where, m_A and m_B are corresponding order of the fringes. If the glass plate is rotated from an initial angle $i_A = 0°$ or when the glass plate is normal to the incident rays then equation 6.8 can be written as

$$i_B = \sqrt{\frac{n}{t}\delta m\lambda} \tag{6.9}$$

where, $\delta m = m_B - m_A$ is the corresponding change in fringe order. Now, In order to introduce an OPD of $\frac{\lambda}{2}$, the change in fringe order δm must be $\frac{1}{2}$. Considering $\lambda = 655$ nm, $n = 1.5$ for glass and $t = 1.15$ mm for a microscopic glass slide

equation 6.9 yields i_B= 0.0206 rad. Considering 1 rad = 57.30°, i_B= 1.2°. Thus, when the microscopic glass plate is rotated by an angle of 1.2°, the intensity of the central fringe will change from bright to dark.

Again, the intensity of an interference fringe is related to the OPD by the following equation

$$I(x,y) = I_1 + I_2 + 2\sqrt{I_1 I_2}\cos(\frac{2\pi}{\lambda}OPD) \tag{6.10}$$

In terms of optical phase difference (Φ)

$$I(x,y) = I_1 + I_2 + 2\sqrt{I_1 I_2}\cos\Phi \tag{6.11}$$

where, $I(x,y)$ is the final intensity of a point with coordinate (x,y) in the plane of observation, I_1 and I_2 are the intensities of the light ray reflected from the top and bottom surface of the glass slide. The OPD between the two interfering rays is related to the incident angle i. When the central fringe of the interference pattern changes from bright (I_{max}) to dark (I_{min}), the OPD between the interfering light rays undergoes a change by $\frac{\lambda}{2}$. As shown above, by varying the incident angle from 0° to 1.2° in the first OPD interval (0 to $\frac{\lambda}{2}$), the intensity of the central fringe can be varied from I_{max} to I_{min}. The variation between I_{max} and I_{min} can be determined in terms grayscale intensity by recording the interferogram digitally and hence, this technique can be used to determine the OPD in an interferometric process. In the present work, a dedicated optical-setup has been designed to form the interferogram and a smartphone camera has been used to record the same.

6.3 Optical layout and fabrication of the designed smartphone based interferometer

Figure 6.2 (a) shows the schematic of the designed smartphone based interferometric system. A laboratory grade diode laser (655 nm, 5 mW) is placed at the focal plane of a plano convex lens (7 mm diameter, focal length 11 mm, Edmund Optics: 32-404) so that the transmitted beam through the lens substitutes for a point source S shown in Figure 6.1. The propagated beam is incident on a 45° inclined 50:50 beam splitter (Edmund Optics: 68-363) to hit nearly perpendicularly on a microscopic glass slide (Ted Pella, Inc. 260441) thickness 1.15 mm.

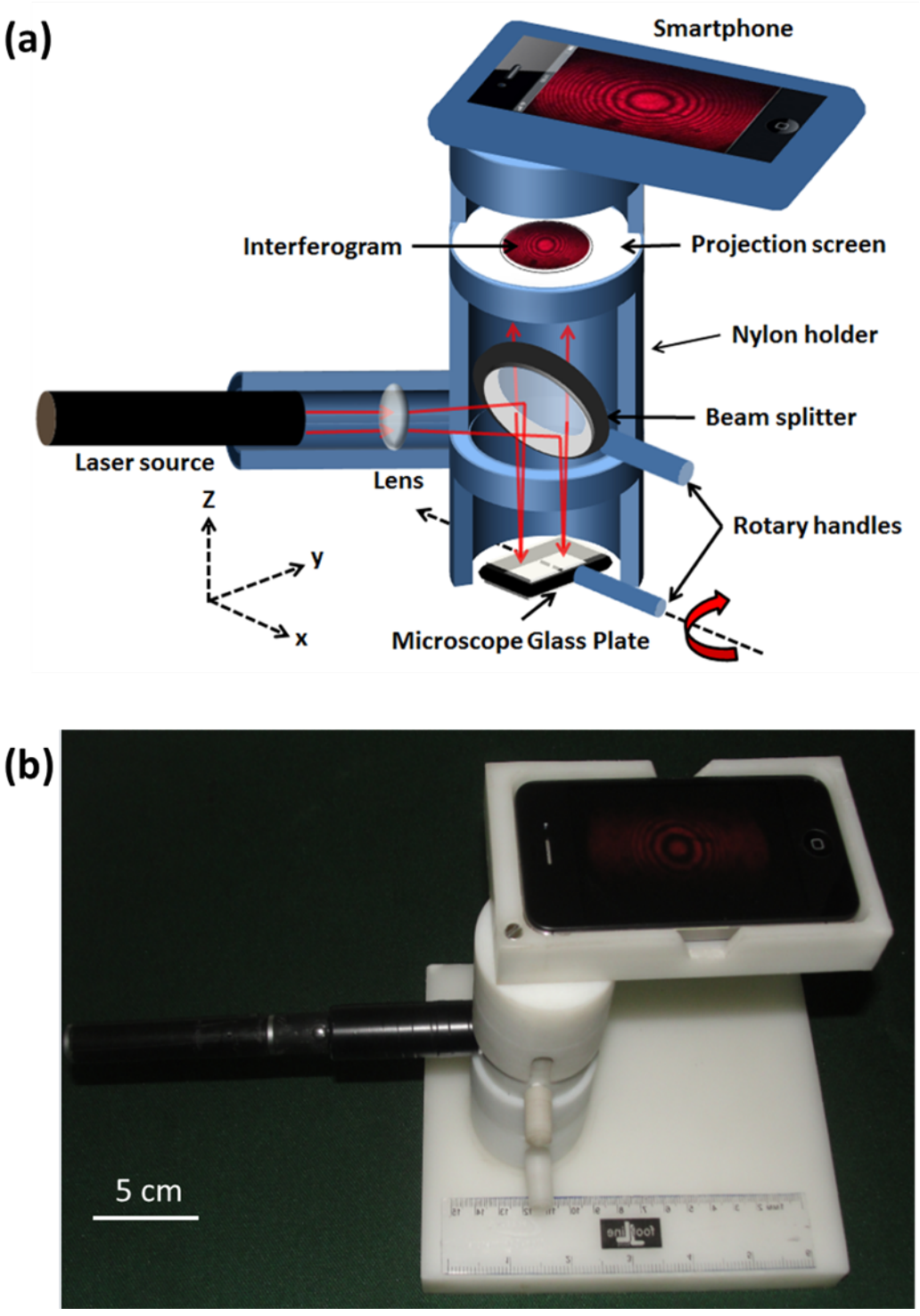

Figure 6.2: (a) Schematic of the designed smartphone based interferometric system and (b) photo image of the designed system.

Part of the incident beam would reflect from the top surface, while the rest would be reflected from the inner bottom face of the glass surface. In the back-reflected light ray there would be an OPD between these two ways which subsequently form

circular interference fringe pattern in the projection screen as shown in Figure 6.2 (a). The smartphone camera has been used to record the the interferogram formed in the screen. In the present work the camera of the Apple iPhone 4 has been used for recording of the interferogram. Technical specifications of this specific phone is summerized in table 6.1 [21].

Table 6.1: Detailed specifications of the iPhone 4 smartphone, apple Inc.

Body	Dimension	115.2 × 58.6 × 9.3 mm
	Weight	137 g
Display	Type	LED-backlit, capacitive touch screen
	Size	3.5 inches
	Resolution	640 × 960 (330 ppi)
Platform	Operating system (OS)	iOS4
	Central processing unit (CPU)	1.8 GHz Cortex-A8
Camera	Primary	5 Megapixels, autofocus
	Sensor size	1/3.2 inches
	Pixel size	1.75 μm
	Focal length	3.85 mm
	Image capture size	2592 × 1936 pixels

All optical components are mounted on a custom-made plastic holder which is made of nylon and blackened it from inside. This plastic material is relatively inexpensive and has high strength and stiffness at elevated temperatures. A rectangular plate has been fabricated by the same material to hold the smartphone so that the camera can directly record the interferogram from the projection screen. Figure 6.2 (b) shows the photo image of the developed smartphone based interferometric system. The glass slide is mounted on a rectangular holder which is attached to a rotary handle. This rotary handle is connected to a micro-positioner so that the glass slide can be rotated with any desired angle.

6.4 Monitoring of optical phase difference in an interferometric process

By turning the laser diode on, the optical platform has been configured to view the circular interference fringes through the smartphone camera. For perfectly

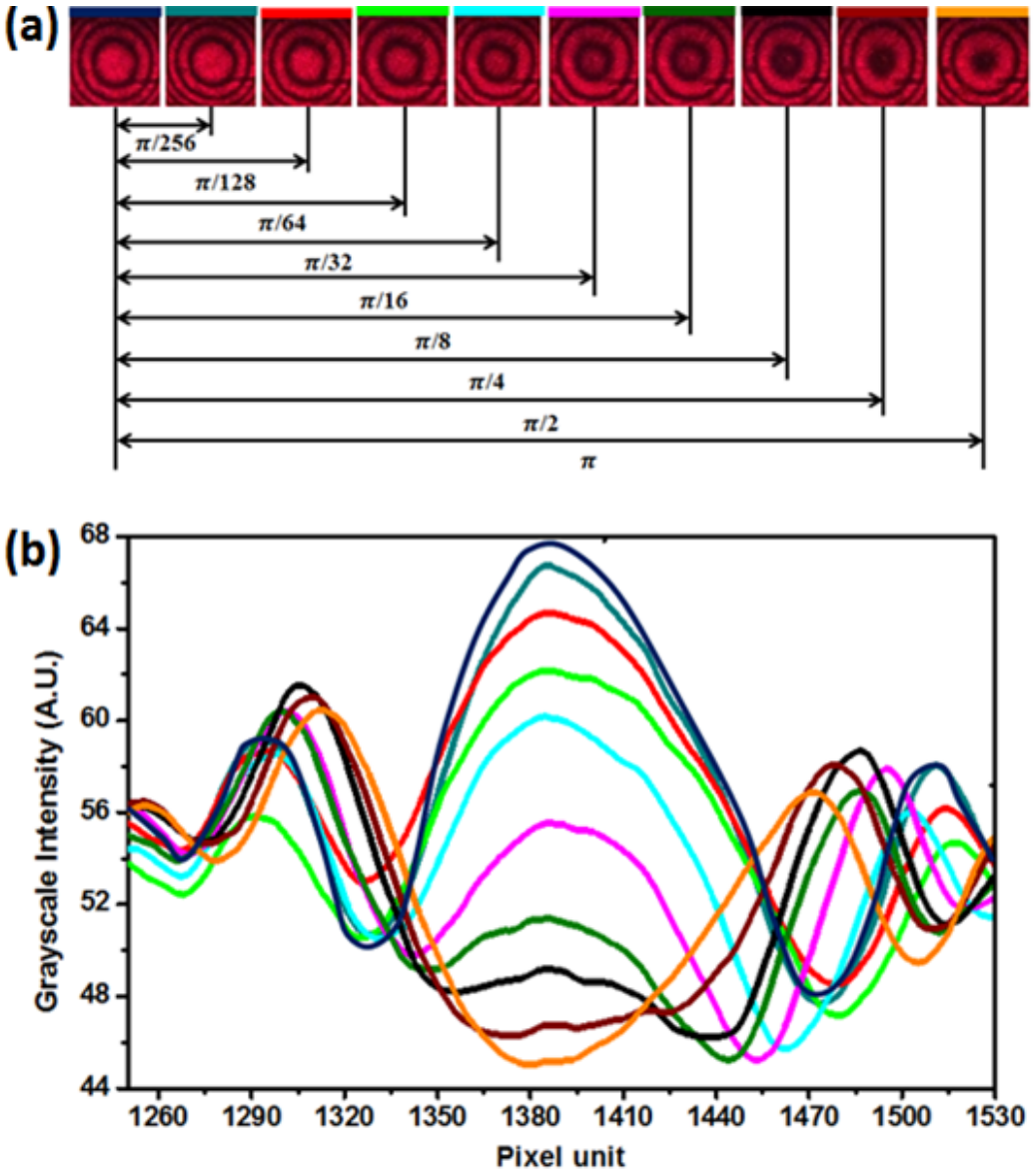

Figure 6.3: (a) Photo image of the captured interferograms and (b) variation of intensity of the central fringe with incident angle.

horizontal position of the slide, the device has been configured in a way that the central fringe coincides with the midpoint of the phone display. The plane of the reflecting glass surface is then gradually rotated so that the incident light beam from the laser hits the glass surface at an inclined angle. Due to inclination, there would be an additional OPD introduced between light beams reflected from the top and bottom surface of the glass slide. Now, the glass slide is rotated in equal steps from 0° to 1.2° to change the central bright fringe (I_{max}) to a dark (I_{min}) state. The corresponding interferogram yield for each angular change has been

captured by the smartphone camera and transfered to a PC. Figure 6.3 (a) shows the cropped images of the captured interferograms when the OPD between the interfering beams changes by $\frac{\lambda}{2}$ or the corresponding phase difference changes by π. In the present study, using the smartphone camera ten distinct stages of interference fringe patterns have been captured. Figure 6.3 (b) shows the corresponding intensity distribution plot of the captured interferogram which clearly indicates the peak intensity value of the central fringe decreases as the optical phase difference between the interfering beams undergo a phase change of π. Considering approximately equal amount of optical phase change occurring between any two neighboring fringe patterns, for the ten different stages the present interferometric system can measure minimum optical phase difference of $\pi/256$. This has been illustrated pictorially in figure 6.3 (a).

The intensity of the fringe pattern of the interferogram depends on the OPD between the two interfering beams. The intensity information can be used to determine the angle of incidence or more specifically the inclination angle of a plane reflecting surface. In the present case the intensity of the central fringe changes from maximum (I_{max}) to its minimum (I_{min}) when the glass slide is rotating by an angle 1.2°. The captured interferograms are cropped to 25 × 25 pixels to consider only the central fringes and then converting into corresponding grayscale value by using the following empirical relation [22]

$$\text{Intensity} = 0.2989\text{*R} + 0.5870\text{*G} + 0.1140\text{*B} \tag{6.12}$$

where R, G, and B are the intensity of the red, green and blue channel of each pixel of the image respectively. Figure 6.4 (a) shows the cropped images of the interferograms which has been labeled with the angle and intensity information. Figure 6.4 (b) shows the characteristic plot of the normalized intensity versus the angular rotation of the glass slide in the first OPD interval from 0 to $\frac{\lambda}{2}$. It has been observed that the variation in intensity of the central fringe with the changes in incident angle is non-linear as predicted by the equation 6.10 and it matches well with 4^{th} order polynomial as shown by red line in the figure. The coefficient of determination $R^2 = 0.995$ signifies that the present optical set-up can be used to determine angular variations accurately and precisely.

The relation between intensity and OPD shown by equation 6.10 is sinusoidal in

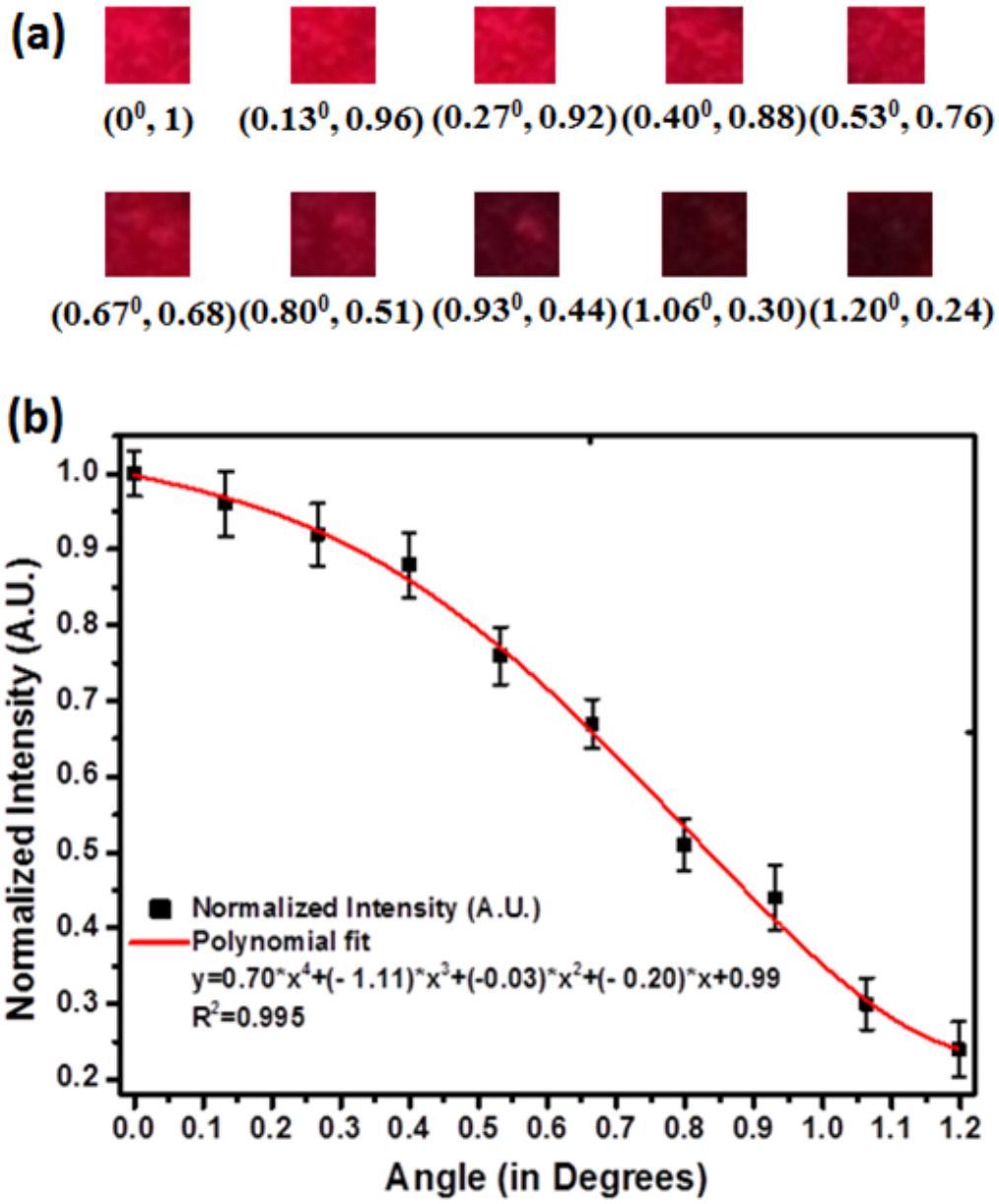

Figure 6.4: (a) Cropped images of the central fringe of the interferograms and (b) Characteristic plot of normalized intensity versus the angular rotations of the glass slide.

nature i.e. for each cycle of $\frac{\lambda}{2}$ OPD, the fringe pattern is brought to an initial condition. Therefore, the method is cannot determine the exact interval of OPD where the intensity variation is taking place. However, it has been observed that the interferogram gradually shifts with the inclination of the reflecting surface and the sense of fringe shifting (+ve or -ve direction) depends on the sense of rotation of the glass slide. In the present work the gradual shift of the fringe

pattern with angualar rotation of the reflecting glass surface has been studied to correlate the order of OPD occuring between the interfering beam with its shift of the interferogram. The need of external computational facility for fringe processing limits the full potential of the system as a portable interferometer for angular measurements. Therefore, the present system has been further redesigned both in its design and required computational facility. In the next section, the development of a fully functional smartphone based interferometric system has been discussed where all the necessary fringe processing can be possible within the smartphone itself through custom developed applications.

6.5 Design of the interferometric optical set-up using 3D printer

With the availability of 3D printer , the interferometric system has been fabricated using this tool. In addition to it, a smartphone application has been developed for onboard fringe processing which makes the the designed interferometric system a standalone platform for sensing investigations. The developed system and the custom designed application are used to determine small angular measurements. Equation 6.9 implies that the change in fringe order of the interferogram (δm) depends on the square of the angle of incidence i_B. It has been experimentally found that the central fringe changes from bright to next bright state when the fringe order is changed by ± 1 in the interferogram. Again, as discussed in the above section, for every OPD interval, the intensity of the central fringe changes from bright (I_{max}) to dark (I_{min}), therefore the intensity information can be used to determine the angular change (θ_I) of the glass slide. However, equation 6.10 shows that the intensity *I (x,y)* of the fringes depends on OPD or on incident angle in a sinusoidal manner as shown in figure 6.5. This means that the same intensity pattern repeats after each cycle of OPD change. As shown in figure 6.5, when the central fringe changes from bright to its next bright state with δm=1, the OPD interval changes from OPD1 to OPD2. Since, the intensity repeats in the same manner for both the intervals, the proper information of a particular OPD interval is crucial to accurately determine the θ_I.

Again, it is observed that with the change in rotational angle, the interferogram

shifts which is attributed to the law of reflection of the light rays from the glass slide. Therefore, for each step increment of OPD by $\frac{\lambda}{2}$, the position of the interferogram shifts toward the direction of rotation in a linear trend. This shift can be determined by processing the

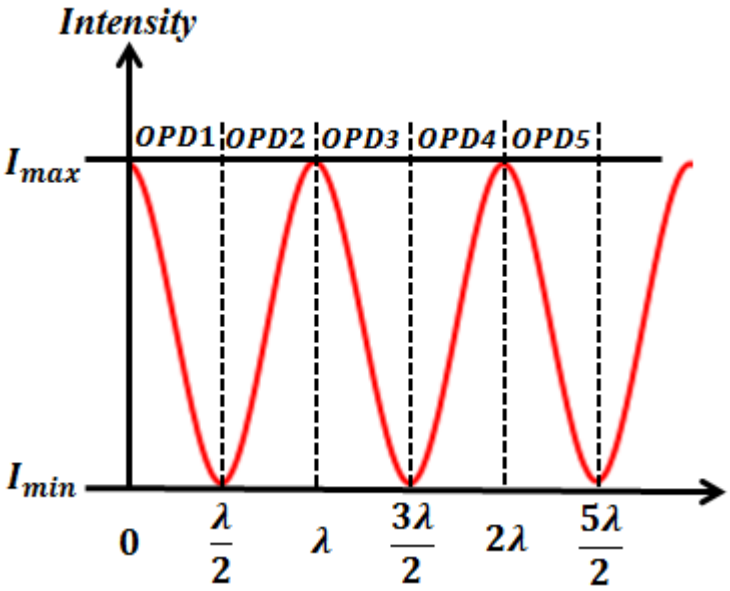

Figure 6.5: Schematic of the optimized experimental set-up for smartphone based interferometric system.

interferogram with the smartphone application and therefore it is possible to determine the corresponding OPD interval. Thus, upon finding the OPD interval, the inclination angle θ_I can be measured. Finally, the total angle can be computed by adding i_B and θ_I. Thus, the total angular rotation of the glass slide can be determined based on the following steps:

1. Determine the change in fringe order δm in order to find angle i_B.

2. Determine the direction of angular measurements: anticlockwise for δm = + ve and clockwise for δm = -ve.

3. Determine the OPD interval by measuring the distance of the center line of the last fringe in the interferogram from the image boundary.

4. Determine the grayscale intensity of the central fringe and compute the small angle θ_I.

5. Compute the final angle, $\Omega = i_B + \theta_I$.

6.5.1 Redesigning of the proposed smartphone interferometer

In this section, the optics design of the previously demonstrated system with the inclusion of spatial filtering assembly in the set-up is discussed. This ensures smooth intensity profile of the incident laser beam and thus improves the signal to noise ratio (S/N) in the interferogram. A diode laser of wavelength (λ) 530 nm is used as a light source which

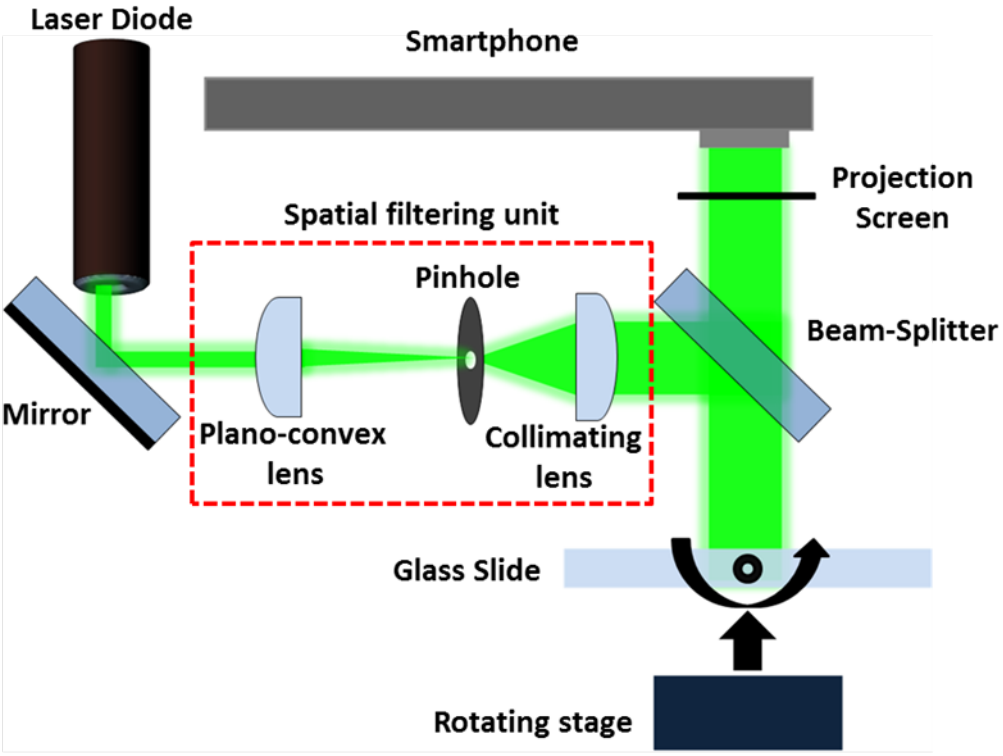

Figure 6.6: Schematic of the optimized experimental set-up for smartphone based interferometric system.

has the beam diameter (D) of 1.6 mm. To determine the spatial filter or pinhole, at first the beam spot diameter has been evaluated using the following empirical formula [23]

$$\text{Beam spot diamter} = \frac{1.27 * \lambda * f}{D} \tag{6.13}$$

In the present case, a plano-convex lens of focal length $f = 75$ mm is used to focus the laser beam, therefore equation 6.13 yields the beam spot diameter as 31.55

μm. Now, the size of the pinhole to be used as a spatial filter can be from using the following relation [23]

$$\text{Pinhole Diameter} = 1.5 \times \text{Beam spot size diameter} \tag{6.14}$$

This yields the required diameter of the pinhole as 47.32 μm. Therefore, for spatial filtering a 50 μm diameter pinhole has been used. A divergent beam of light from the spatial filter is collimated by a plano-convex lens (focal length 11 mm, diameter 7 mm). Figure 6.6 shows the schematic of the optical system where the spatial filtering unit has been indicated in it. Similar to the earlier work, by using a 50:50 beam splitter the collimated light beam is allowed to incident normally on the microscopic glass slide and the generated circular interference fringe pattern is projected on a screen. For the present investigation, the rear camera of the smartphone (Samsung Galaxy J7 prime with 13 Megapixel camera) has been used to capture the interferogram. The detailed specification of the phone is given in the table form 6.2 [24].

Table 6.2: Detailed specifications of the Samsung Galaxy J7 prime smartphone

Body	Dimension	151.7 × 75 × 8 mm
	Weight	167 g
Display	Type	TFT capacitive touchscreen
	Size	5.5 inches
	Resolution	1080 × 1920 (330 ppi)
Platform	Operating system (OS)	Android 7.0 (Nougat)
	Central processing unit (CPU)	Octa-core 1.6 GHz Cortex-A53
Camera	Primary	13 Megapixels, autofocus
	Sensor size	1/3.1 inches
	Pixel size	1.12 μm
	Focal length	3.7 mm
	Image capture size	4802 × 3120 pixels

All the opto-mechanical components required to develop the proposed smartphone interferometric system have been designed with the licensed ZW3D CAD modeling software shown in figure 6.7 (a) and then fabricated through FFF printing technology in a 3D printer (Raise N2 Plus). This 3D printer has a layer resolution of 10 μm in the Z-direction and 12.5 μm X/Y step size assures best print quality

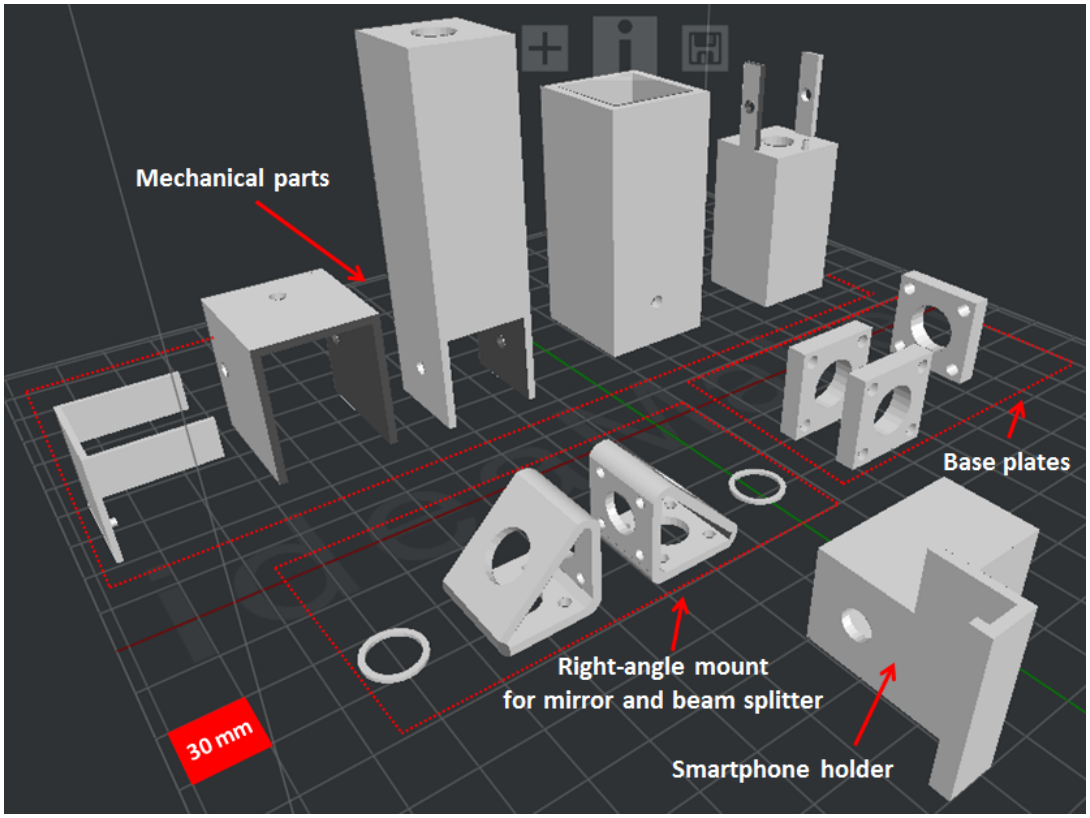

Figure 6.7: Different opto-mechanical components printed to develop the 3D printed interferometric system.

and accuracy. For the present work, ABS thermoplastic polymer filament has been considered as a printing material. Prior to start the printing process all the required printing parameters have been set by using licensed ideaMaker software and the designed models have been sliced accordingly. To get a rigid strength and durability of the designed opto-mechanical parts, the infill density has been set as 45% during printing of the different parts. The customized mechanical parts have been designed in the required sizes to hold the laser, projection screen, right angle mounts and the base plates. Figure 6.8(a) shows the complete 3D model of the designed smartphone interferometer system. All optical components such as lens and pinhole etc. have been mounted to the respective 3D printed parts and finally assembled using M3 cap screws (Product id: SH3M5, Thorlabs). Figure 6.8(b) shows the photo image of the designed smartphone interferometric system. Use of 3D printed opto-mechanical parts eventually reduces the overall fabrication cost. The whole system has been fabricated using black 3D printer filament which eventually blocks almost any external light interference. One of the main

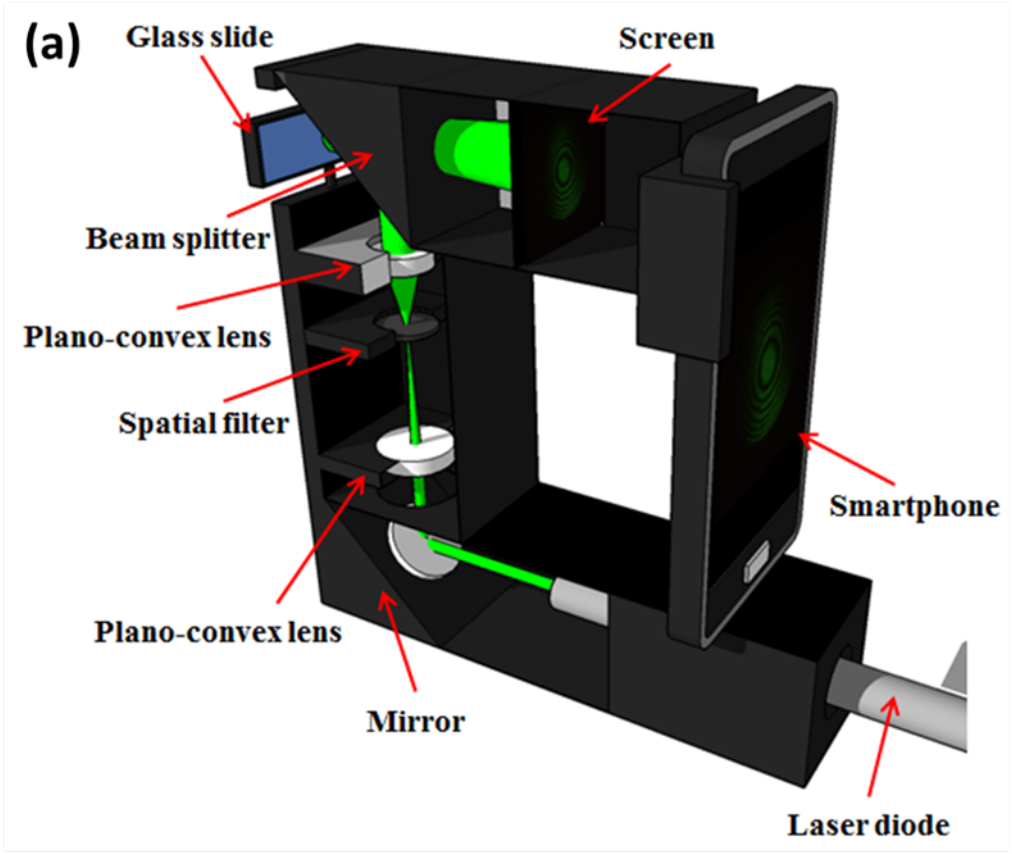

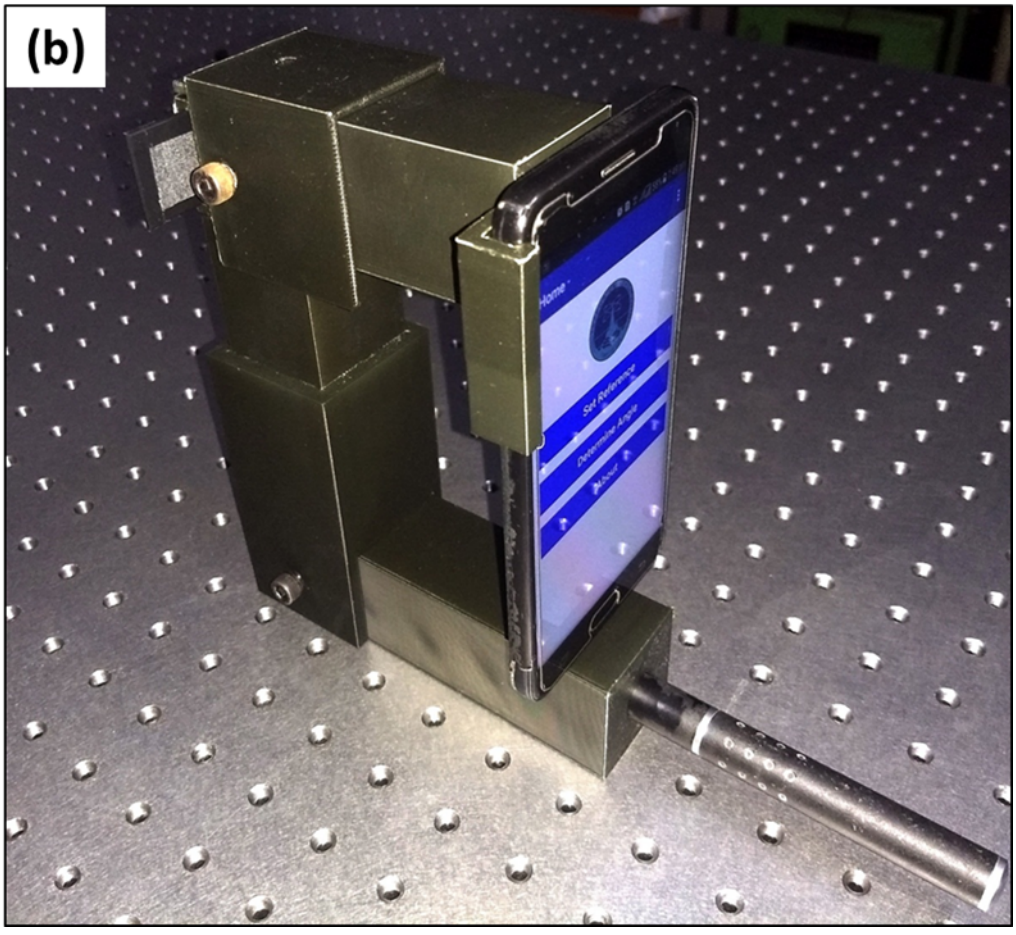

Figure 6.8: (a) 3D design of the smartphone based interferometric system and (b) photo image of developed system.

objectives of the proposed work is to develop necessary computational platform for fringe analysis within the smartphone. Therefore, an android application has also been developed for onboard fringe processing and automatic evaluation of angular rotation of the glass slide. Details about the development of the custom designed application and different image processing algorithms used for the present work have been discussed in the next section.

6.5.2 Smartphone application based fringe processing and data analysis

In the present study, **FringeApp** - an android platform based application has been developed for automatic fringe processing and data analysis. The application has been developed using freely available integrated development environment (IDE), Android Studio software [25]. For automatic fringe processing, the OpenCV image processing library has been incorporated in the Android software development environment and required algorithms have been implemented [26]. For the considered smartphone, the interferogram is recorded as a two-dimensional (2D) image in jpg format with size 4128 x 3096 pixels. The recorded interferogram can be converted to a one-dimensional (1D) image through onboard image cropping facility developed within the smartphone application and this reduce the processing time sufficiently. The consideration of single pixels or a line-cut of the interferogram for data analysis can significantly increase the measurement error while determining the intensity of the central fringe. This particular smartphone is embedded with a 1.6 GHz Octa-core central processing unit (CPU) which is sufficient enough to handle more complex image processing algorithms. Therefore, for the present case to evaluate the intensity of the central fringe, the pixel averaging algorithm over a 2D interferogram has been implemented within the same application. Considering the high-end image processing capability of the smartphone, all image processing algorithms used for automatic fringe processing have been implemented through calling specific functions from the OpenCV image processing library in a certain order shown in figure 6.9. After converting the interferogram to the corresponding grayscale image, initially a 3 x 3 median filter has been used twice to remove the speckle noises which may be present due to the high intensity of the laser source.

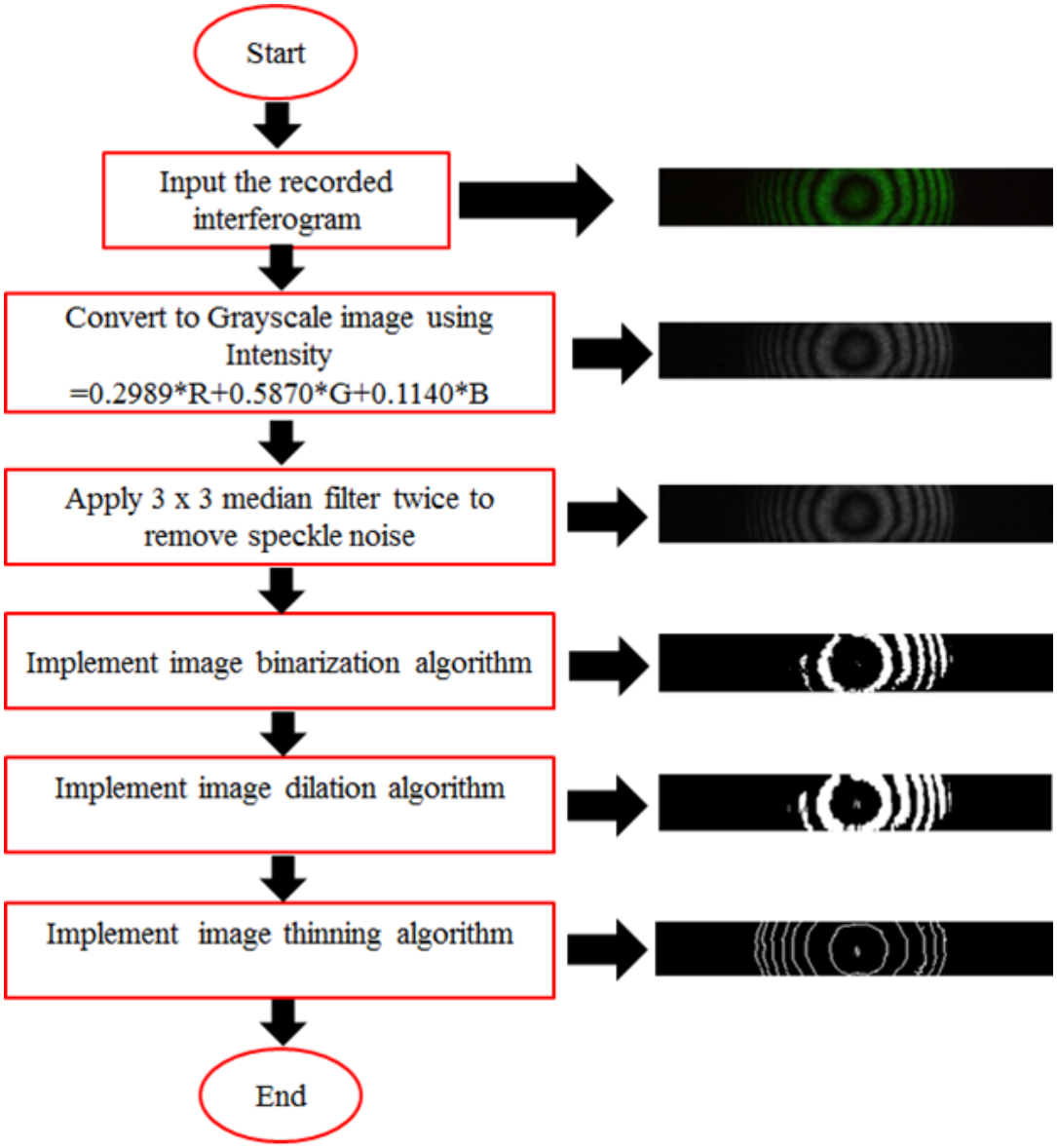

Figure 6.9: Detailed workflow of the image processing algorithms implemented in the **FringeApp** application.

Following the existing fringe processing techniques [27,28], the filtered interferogram has been converted to its binary form by using the widely used Otsus thresholding method [29]. In this particular method, at first the threshold level has been chosen iteratively and fixed at 0.17 where the fringes become comparatively distinct. It has been found that there are many unconnected pixels in the binary image which may occur due to non-uniform illumination. To mitigate this issue, the image dilation algorithm has been implemented so as to connect and fill the missing pixels with a line structuring element. After generating the di-

lated binary image as shown in figure 6.9, the image thinning algorithm has been implemented to get the fringe center lines. The fringe center line is consisting of pixels with 8-neighborhood connections therefore on implementing a tree search algorithm [30], all the pixels bearing to a single fringe center line can be grouped and the respective order can be assigned. Since, the white pixels in the fringe center lines have the same intensity value; therefore a simple line scan for intensity values through the central fringe could yield the same result. because only pixels bearing to a particular fringe center line can produce an intensity peak. This simple algorithm has been implemented in the **FringeApp** application.

At the beginning a user needs to set the optical set-up so that the glass slide is perpendicular to the incident light beam. This ensures 0° as the reference angle. With this configuration, user needs to run the **FringeApp** application to record the reference interferogram by clicking the 'Capture Reference' button. The developed application will capture the interferogram and crop it to a dimension 302 pixels x 95 pixels shown in figure 6.10 (a). Now, the user needs to click the 'Process Reference' button to process the reference interferogram. Upon clicking this button, the application will implement all the considered image processing algorithms in the background and process the interferogram shown in figure 6.9 which contains the fringe center lines. The overall processing time taken by the smartphone is around three minutes. For high end CPU configuration smartphone, the processing time can be improved. The reference interferogram is stored in the application interface as canvas for further use. For any arbitrary angular rotation of the glass slide, it will generate a characteristic interferogram. To determine the arbitrary angle, user needs to click the 'Capture Interferogram' button which will capture and crop the interferogram to the desired dimension. Similarly, on clicking the 'Process Interferogram' button the application will process the interferogram to yield the desired interferogram with fringe center lines. Now, using the sliders as shown in figure 6.10 (a), user needs to select the 0th order fringe pattern in the processed interferograms and 25×25 pixel image area of the central fringe of the raw interferogram. The user then needs to click the 'Determine Angle' button to automatically determine the corresponding angle. Upon clicking this button, the **FringeApp** will scan through middle of the processed interferogram to determine intensity peaks. Since, only the fringe center line has the brightest pixels, therefore

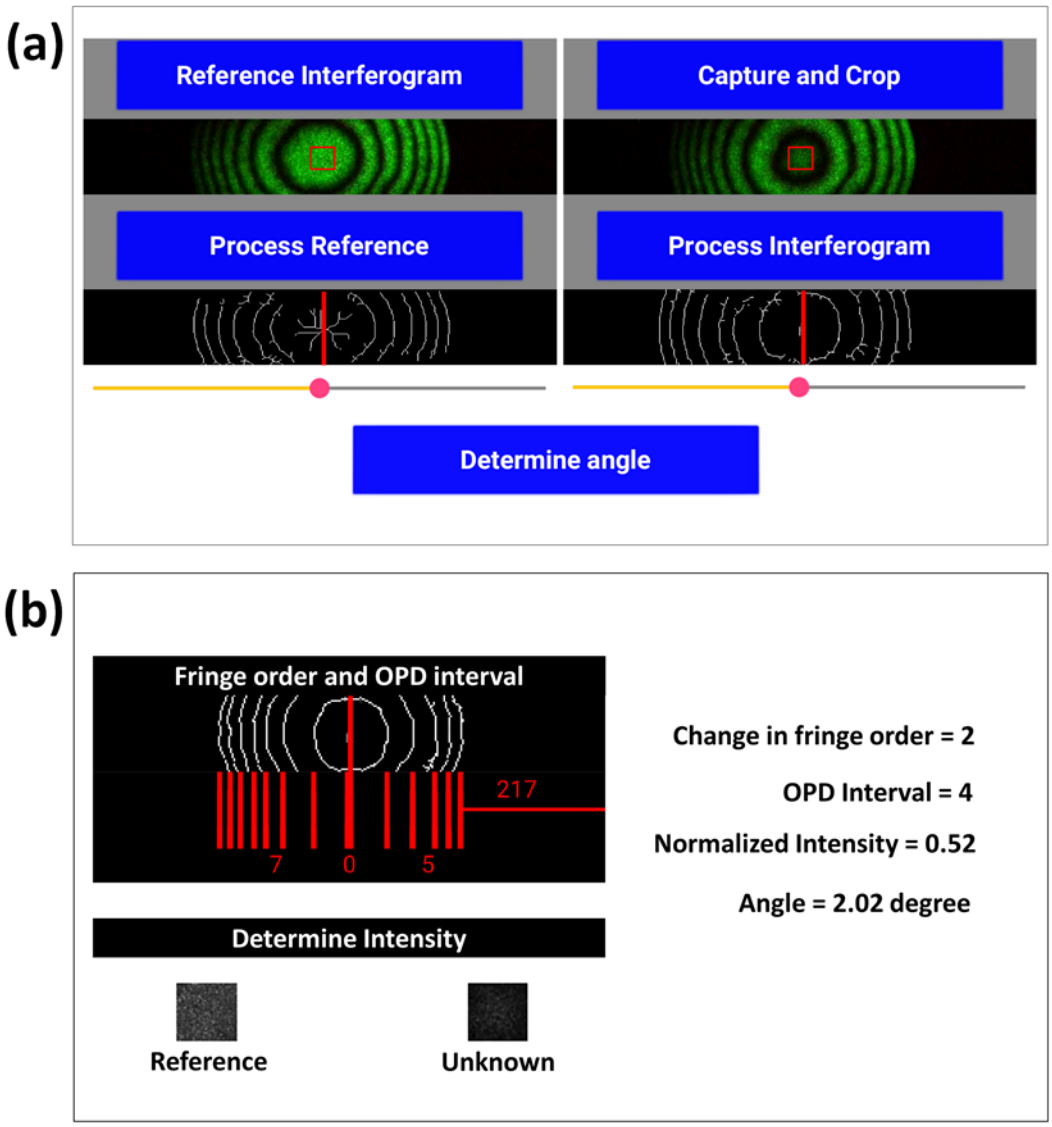

Figure 6.10: (a) Screenshot images of the first window of the designed FringeApp application showing the reference and the interferogram with arbitrary angle and (b) screenshot image of the detection window developed for automatic fringe processing and evaluation of the angular rotation.

the application will record intensity peaks at the positions of the interferogram containing the fringe center line only as shown in figure 6.10(b). Then the application will automatically count the number of fringe center lines in both sides of the 0th order fringe of the interferogram with unknown angle and determine the distance of the last fringe center line from the image boundary. After this task, the application will automatically crop the 25 $\times$ 25 pixels selected area of the central fringe of both the reference and captured interferogram and convert them

into the corresponding grayscale values and to evaluate the normalized intensity of the interferogram for unknown rotational angle of the glass slide. The normalized intensity value has been evaluated by dividing the intensity of the interferogram of unknown angle by the intensity of the central fringe of the reference interferogram. Upon evaluating all the parameters, the designed smartphone application will automatically compute the resultant angle as shown in figure 6.10(b).

6.5.3 Determination of small angular rotations by the interferometric system

The performance of the designed system has been investigated for detection of small angular rotation of the glass slide. In the present case, with λ=530 nm, $n = 1.5$ for glass and $t = 1.15$ mm for a microscopic glass slide equation 6.9 shows that the intensity of the central fringe changes from bright (I_{max}) to next bright state (I_{max}) with $\delta m = 1$ for i_B=1.50°. With this argument, considering $\delta m = \frac{1}{2}$ when the central fringe changes from bright (I_{max}) to dark state (I_{min}) in the first OPD interval, the corresponding angular rotation is estimated to be i_B=1.06°. Similarly, for all the angles within the detection range, the angular rotation can be estimated using equation 6.9.

The workability of the optimized smartphone based interferometric system has been demonstrated in measuring of small angular change by rotating the microscopic glass slide with XYZ Translation Stage (0.5 mm translations per revolution). At first, the glass slide is made normal to the incident beam so that the angle of incident becomes 0°. This configuration has been considered as reference for all the measurements where the fringe order (δm) is 0. The corresponding interferogram generated for 0° is captured by the smartphone camera and processed by **FringeApp** application to get the fringe center lines. Both the raw and processed interferogram are stored in the phone internal storage for further use as a reference as discussed in the fringe processing section. Now, one side of the glass slide is attached to the stage by a hook so that when the stage is translated by 0.01 mm in the Z - direction, the glass slide is rotated in steps of $\tan^{-1}(\frac{0.01mm}{37.5mm})$= 0.02° about an axis passing through the middle of the glass slide where 37.5 mm is the distance between the middle of the glass slide to the hook. The corresponding

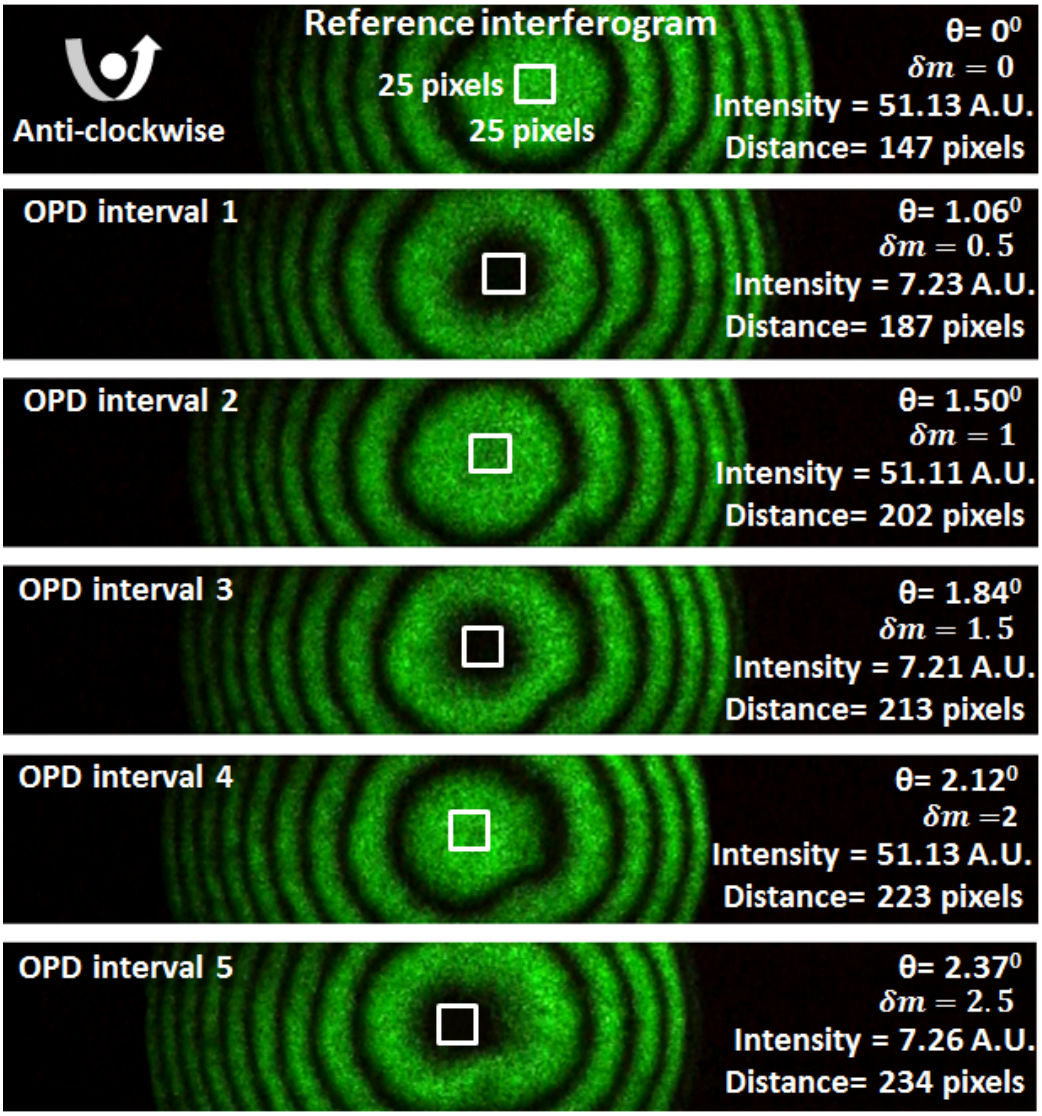

Figure 6.11: Photo images of the captured interferogram for different OPD intervals.

interferograms has been recorded by the smartphone camera and processed by the smartphone applications to determine the change in fringe order, OPD interval and the grayscale intensity of the central fringe as discussed in subsection 6.5.2. Figure 6.11 shows the examples of the interferograms recorded by the developed smartphone based system for five different OPD intervals. The figure clearly indicate observe that the interferograms translate towards left with nearly in equal steps when the glass plate is rotated in the anticlockwise direction.As shown in the figure, a 25 $\times$ 25 pixels area of the interferogram is used to determine the intensity of the central fringe. The captured interferograms have been processed by the application to get the fringe center lines and the distance of the last fringe

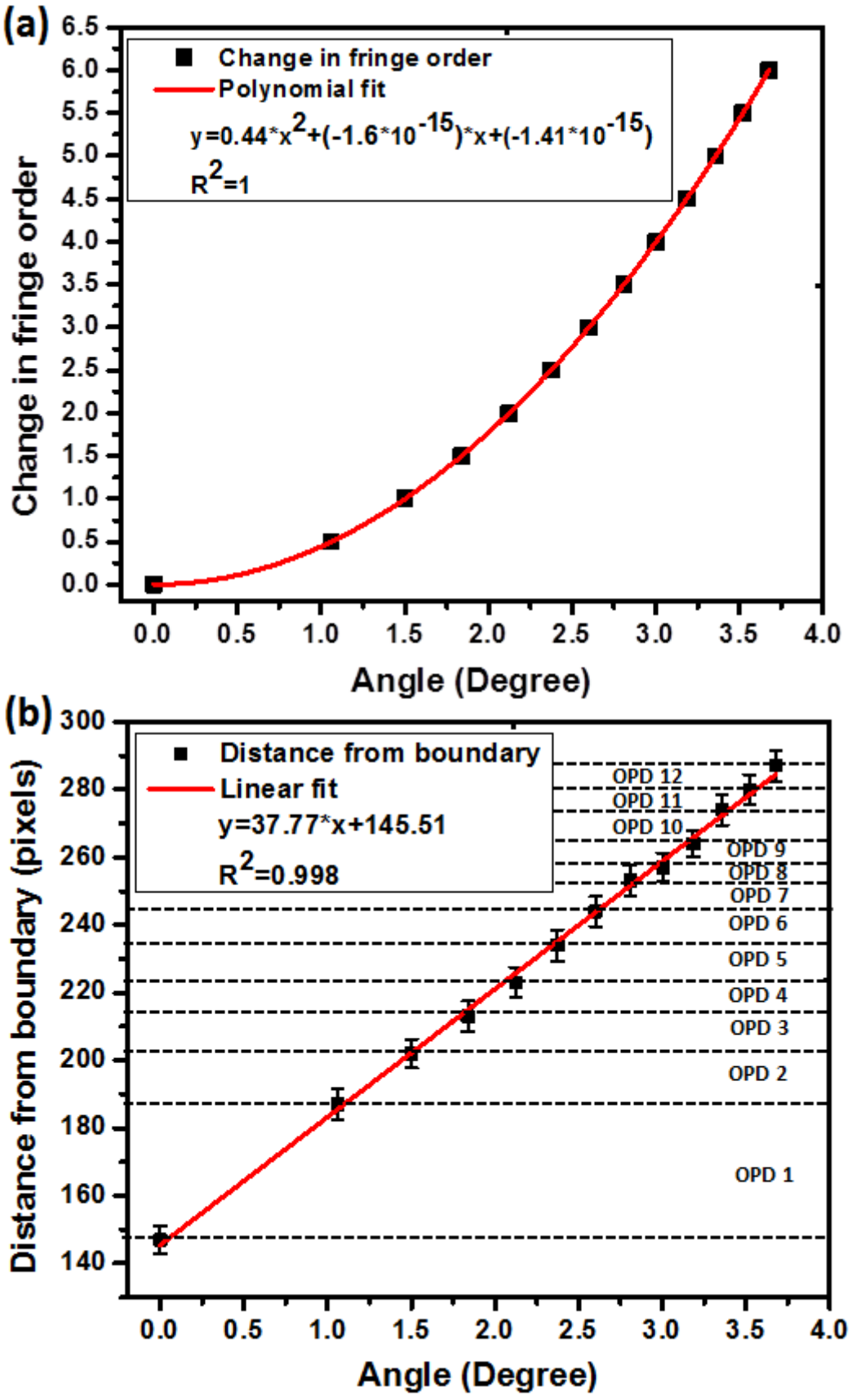

Figure 6.12: (a) variation of fringe order and (b) variation of distance of the fringe center line from the boundary of the interferogram with the angular rotation of the glass slide.

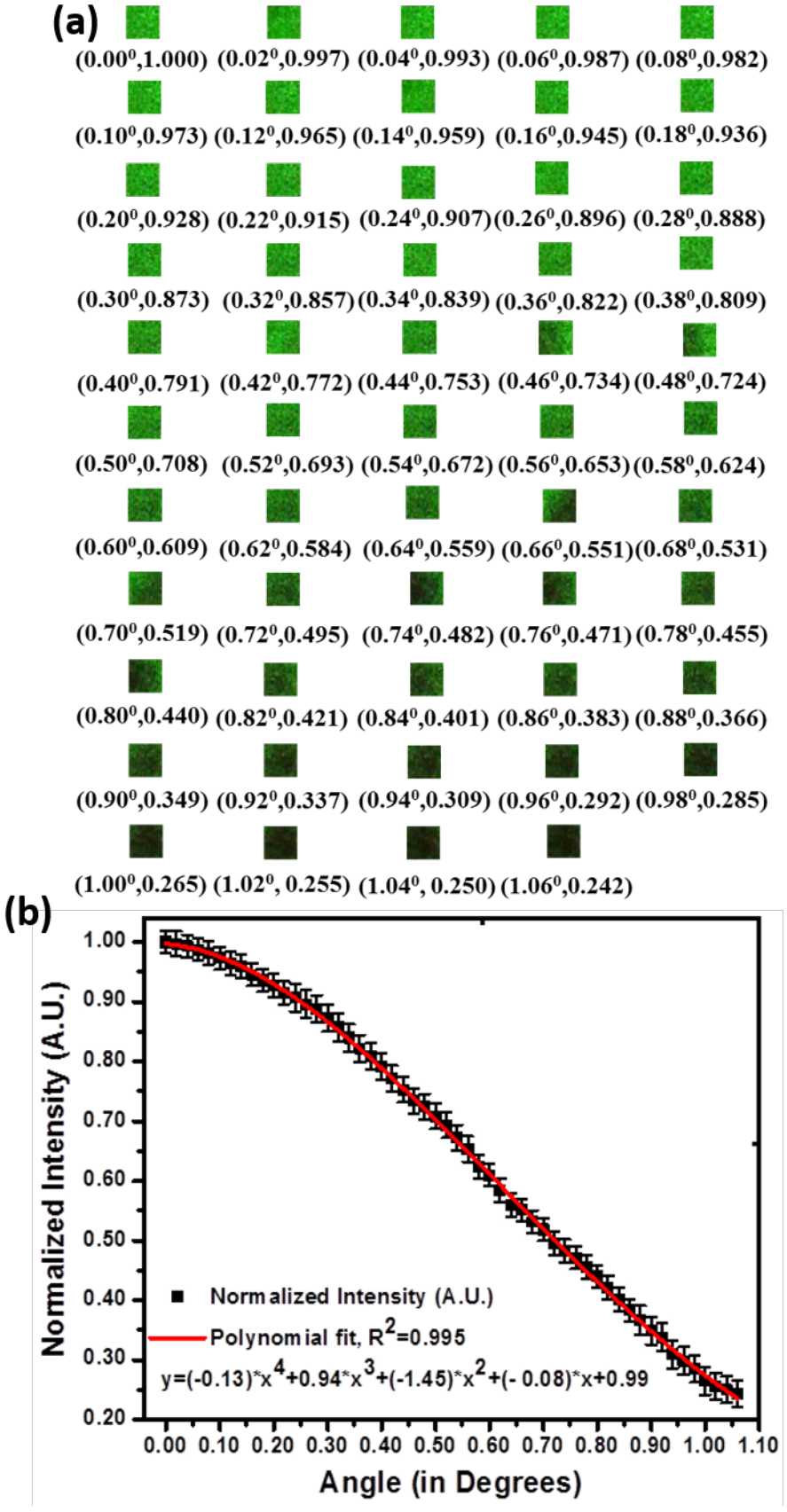

Figure 6.13: (a) Cropped photo images of the central fringes when the glass slide is rotated with a step of 0.02° and (b) characteristic plot of normalized intensity versus the angular rotations of the glass slide in the first OPD interval.

center line of the processed interferogram from the image boundary. Figure 6.12 (a) and figure 6.12 (b) shows the characteristic plot of the variation of fringe order and shift of the interferogram with the angular rotation of the glass slide. As shown in figure 6.12 (b), the distance of the fringe center line from the boundary of the interferogram has been divided into its corresponding OPD intervals. With this data, a look out table has been obtained within the **FringeApp** application to determine the OPD interval based on the calculated distance for an arbitrary angular measurement of the reflecting surface.

When the central fringe changes from bright (0°) to dark (1.06°) in the first OPD interval the intensity will change from I_{max} and I_{max} shown in figure 6.11. In the first OPD interval, the change in intensity value of the central fringe when the glass slide is rotated by in steps of 0.02° has been determined by using a 25 × 25 pixel area of the central fringe. Figure 6.13 (a) shows the cropped images of the central fringe labeled with the respective angle and normalized intensity values. A distinct variation in intensity value has been observed with the increase of the angle. Figure 6. 13(b) shows the corresponding characteristic plot of the normalized intensity versus the angular rotation of the glass slide in the first OPD interval. It has been observed from figure 6.13(b) that the variation of intensity of the central fringe with the incident angle is non-linear as predicted by the equation 6.10 and exactly matches with 4^{th} order polynomial with coefficient of determination $R^2 = 0.995$. This calibration curve has been implemented in the **FringeApp** application for further use. Since, the OPD interval is non-linear with the angular change, therefore for each OPD interval different characteristic curves have been developed. Figure 6.14 shows the response characteristic of four OPD intervals: OPD 2 (1.06° to 1.50°), OPD 3 (1.50° to 1.84°), OPD 4 (1.84° to 2.12°) and OPD 5 (2.12° to 2.38°) when the glass plate is rotated in step incremental angle of 0.02°. The response of the smartphone interferometric system in all these OPD intervals have been found to be nonlinear as predicted by the theory. All these nonlinear fitted curves have been implemented in the **FringeApp** for determination of unknown angular rotation of the glass slide.

The sensitivity of the designed smartphone based system in measuring of small angles is primarily depending on the capability of the smartphone camera module in distinguishing small change in intensity of the central fringe. Due to the

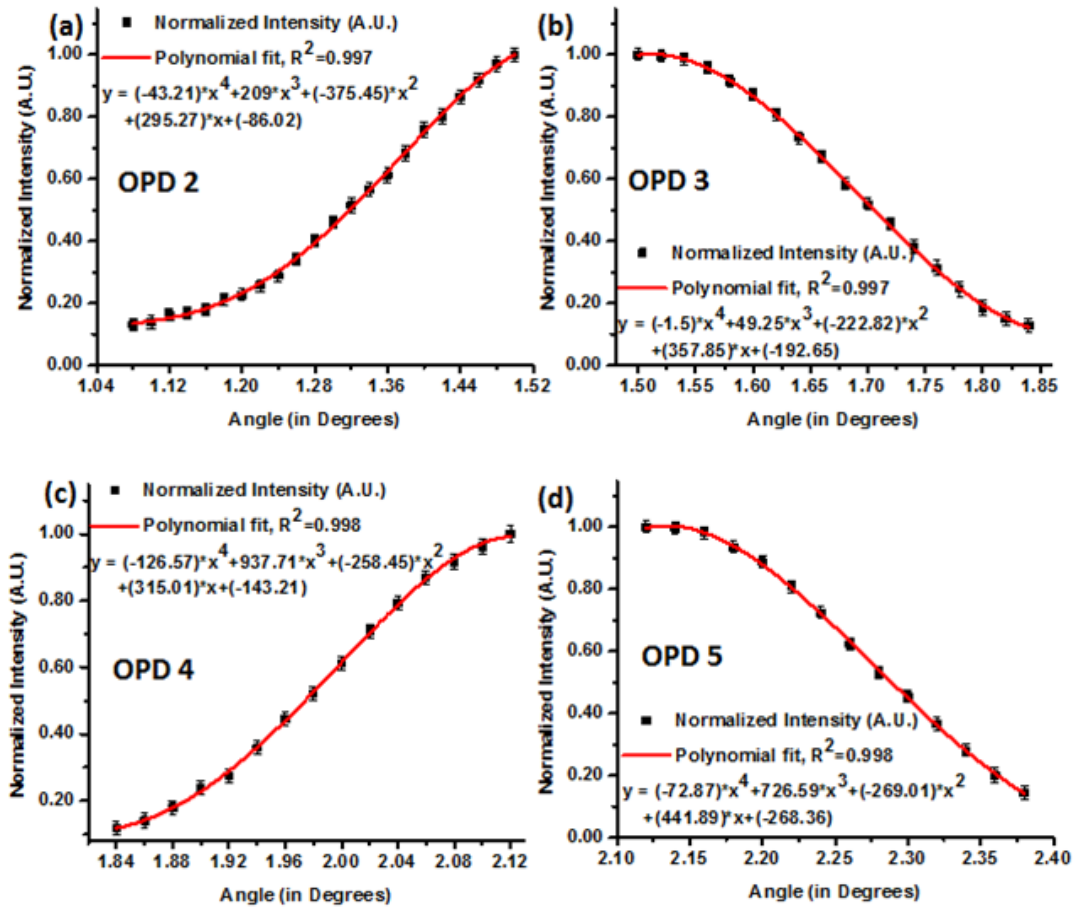

Figure 6.14: The characteristic plots of intensity versus angular rotation of the glass slide for different OPD intervals.

nonlinear response characteristic, the sensitivity has been measured as an average sensitivity for three linear regions in the fitted curves which has been shown in figure 6.15. The sensitivity of the smartphone based interferometric system in the first OPD interval is found to be 0.65 A.U./degree.

The dynamic range in measuring angles by the present device is limited by the optical design and the camera resolution. The present smartphone interferometric system can measure angular variations as low as 0.02° which is limited by the calibration steps provided by the micro-positioner. Since, the most of the smartphone camera has a resolution of 8-bit or it can distinguish 256 gray levels therefore with more sophistication in the device it is possible measure angular change as low as 0.004°.The number of fringes formed in the interferogram plays a critical role to provide the maximum angular rotation that the designed system can measure. With the present optical set-up, the maximum fringes formed in the interferogram

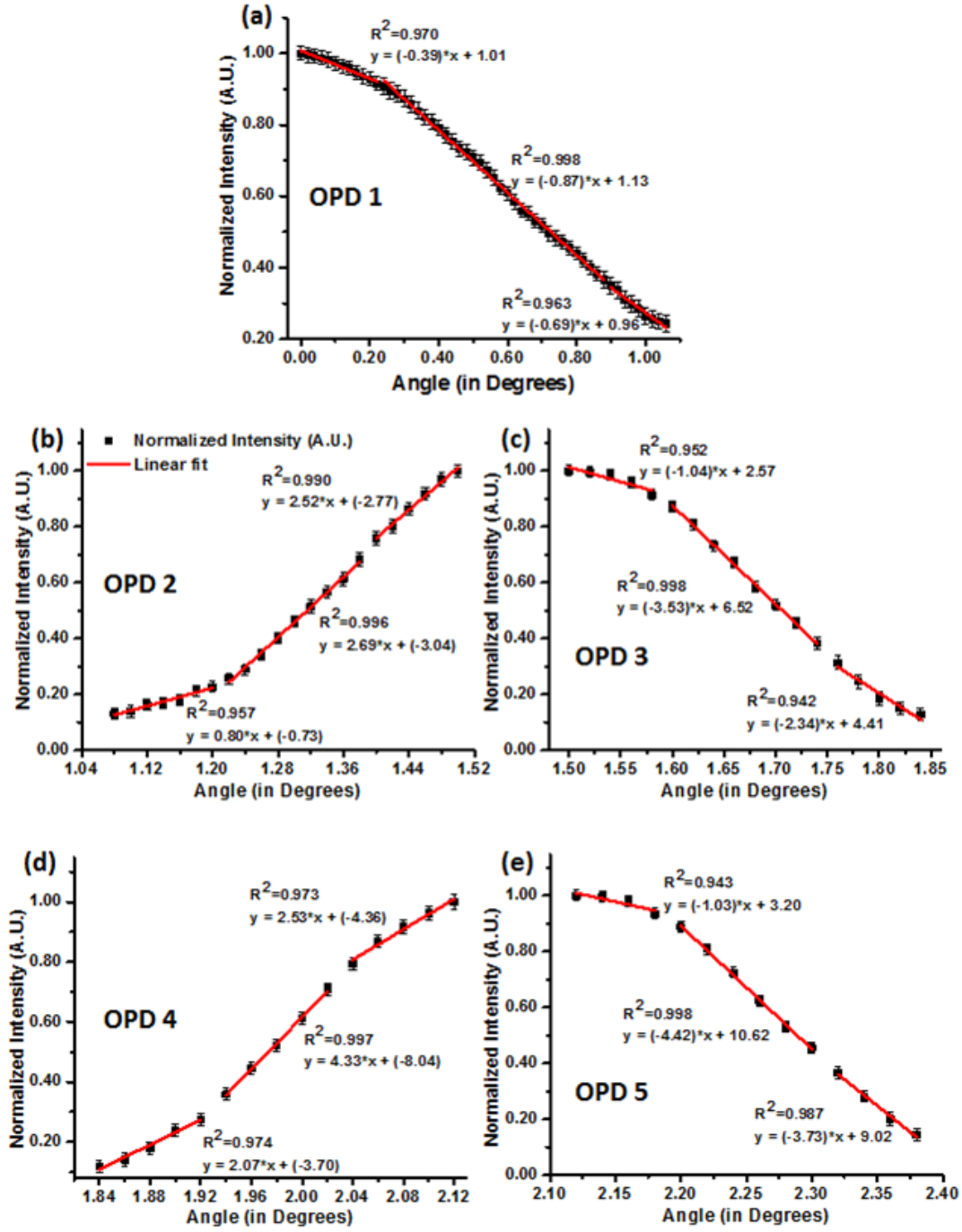

Figure 6.15: Linear fitting of the intensity versus angular rotation of the glass slide for different OPD intervals.

has been limited to six which limits the maximum measurable angle to ± 3.68 °. Therefore, the dynamic range of the designed smartphone based interferometric system is ±3.68 °. The interferometric technique has been primarily developed for ultra small angular measurements which cannot be possible by conventional mechanical devices. As compared to its commercially available counterparts, the

proposed smartphone platform technique offers several advantages in terms of field-portability, relatively easy to handle, fully automated, ability to share in-field data from remote location along with cost efficiency.

6.6 Summary

In summary, this chapter describes the usability of a modern smartphone for interferometric based metrological applications. The camera of the smartphone has been used as a detector for recording of the interferograms. Besides, the usability of the smartphone as a recording media, a computational platform has been developed for fringe processing and analysis of the interferogram. The onboard fringe processing capability of the smartphone makes the proposed platform a standalone tool. Besides, the optical part, all the needed mechanical components required for optics holding has been fabricated using 3D printing technology. The use of 3D holderoffers advantages in terms of flexibility of the design, robustness of fabrication at a low cost approach over its commercial counterparts. The smartphone interferometric system has been used to monitor change in phase difference in an interferometric process and later with proper optimization of the design it has been used to measure small angular rotations (0.02°). In future, the applicability of the proposed device will be demonstrated for more complex interferometric based applications such as determination of thin film thickness, refractive index etc.

References

[1] Sirohi R. S. *Introduction to Optical Metrology*,CRC Press, London,2015.

[2] Monnier, J.D. Optical interferometry in astronomy. *Reports on Progress in Physics*, 66(5):789, 2003.

[3] Rao, Y.J. Recent progress in fiber-optic extrinsic FabryPerot interferometric sensors. *Optical Fiber Technology*, 12(3):227-237, 2006..

[4] Schreiber, K.U., Hautmann, J.N., Velikoseltsev, A., Wassermann, J., Igel, H., Otero, J., Vernon, F. and Wells, J.P. Ring laser measurements of ground

rotations for seismology. *Bulletin of the Seismological Society of America*, 99(2B):1190-1198, 2009..

[5] Vakhtin, A.B., Peterson, K.A., Wood, W.R. and Kane, D.J. Differential spectral interferometry: an imaging technique for biomedical applications. *Optics Letters*, 28(15):1332-1334, 2003.

[6] Malacara D. *Optical Shop Testing* ,wiley,New Jersey,2007.

[7] Hariharan, P. *Optical Interferometry*,Elsevier,Netherland,2003.

[8] Wang, Y., Xie, F., Ma, S. and Dong, L. Review of surface profile measurement techniques based on optical interferometry. *Optics and Lasers in Engineering*, 93:164-170, 2017.

[9] Protopopov, V., Cho, S., Kim, K., Lee, S. and Kim, H. Differential heterodyne interferometer for measuring thickness of glass panels. *Review of Scientific Instruments*, 78(7):076101, 2007.

[10] Bobroff, N. Recent advances in displacement measuring interferometry. *Measurement Science and Technology*, 4(9):907, 1993.

[11] Kim, J.A., Kim, J.W., Kang, C.S., Jin, J. and Lee, J.Y. An interferometric system for measuring thickness of parallel glass plates without 2 ambiguity using phase analysis of quadrature Haidinger fringes. *Review of Scientific Instruments*, 88(5):055108, 2017.

[12] Gauglitz, G., Brecht, A., Kraus, G. and Mahm, W. Chemical and biochemical sensors based on interferometry at thin (multi-) layers. *Sensors and Actuators B: Chemical*, 11(1-3):21-27, 1993.

[13] Mariani, S., Strambini, L.M. and Barillaro, G. Femtomole detection of proteins using a label-free nanostructured porous silicon interferometer for perspective ultrasensitive biosensing. *Analytical chemistry*, 88(17):8502-8509, 2016.

[14] Hu, P., Dong, X., Ni, K., Chen, L.H., Wong, W.C. and Chan, C.C. Sensitivity-enhanced Michelson interferometric humidity sensor with waist-enlarged fiber bitaper. *Sensors and Actuators B: Chemical*, 194:180-184, 2014.

[15] Contreras Naranjo, J. C., Wei, Q., and Ozcan, A. Mobile phone based microscopy, sensing, and diagnostics. *IEEE Journal of Selected Topics in Quantum Electronics*, 22(3):1-14, 2016.

[16] Wilkes, T.C., McGonigle, A.J., Willmott, J.R., Pering, T.D. and Cook, J.M. Low-cost 3D printed 1 nm resolution smartphone sensor-based spectrometer: Instrument design and application in ultraviolet spectroscopy. *Optics letters*, 42(21):4323-4326, 2017.

[17] Wei, Q., Luo, W., Chiang, S., Kappel, T., Mejia, C., Tseng, D., Chan, R.Y.L., Yan, E., Qi, H., Shabbir, F. and Ozkan, H. Imaging and sizing of single DNA molecules on a mobile phone. *ACS nano*, 8(12):12725-12733, 2014.

[18] Hossain, M.A., Canning, J., Cook, K. and Jamalipour, A. Smartphone laser beam spatial profiler. *Optics letters*, 40(22):5156-5159, 2015.

[19] Zhang, C., Anzalone, N.C., Faria, R.P. and Pearce, J.M. Open-source 3D-printable optics equipment. *PloS one*, 8(3):e59840, 2013.

[20] Pirnstill, C.W. and Cot, G.L. Malaria diagnosis using a mobile phone polarized microscope. *Scientific reports*, 5:13368, 2015.

[21] Device specifications. *Apple iPhone 4*. Retrieved on 19 Jan. 2018 from https://www.devicespecifications.com/en/model/710a272e, 2018.

[22] Schanda, J. *Colorimetry: understanding the CIE system*,John Wiley and Sons,New Jersey,2003.

[23] Understanding spatial filter.Retrieved on 19 Jan. 2018 from https://www.edmundoptics.com/resources/understanding-spatial-filters/,2018.

[24] Device specifications. *Samsung Galaxy J7 Prime*. Retrieved on 19 Jan. 2018 from https://www.devicespecifications.com/en/model/a3743534, 2018.

[25] Android Studio. *Integrated development environment (IDE)*. Retrieved on 02 JUne. 2018 from https://developer.android.com/studio/ ,2018.

[26] OpenCV library for Android.Retrieved on 02 JUne. 2018 from https://opencv.org/platforms/android/,2018.

[27] Sirkis, J.S., Chen, Y.M., Singh, H. and Cheng, A.Y. Computerized optical fringe pattern analysis in photomechanics: a review. *Optical engineering*, 31(2):304-315, 1992.

[28] Chen, T.Y. and Taylor, C.E. Computerized fringe analysis in photomechanics. *Experimental Mechanics*, 29(3):323-329, 1989.

[29] Otsu, N. A threshold selection method from gray-level histograms. *IEEE transactions on systems, man, and cybernetics*, 9(1):62-66, 1979.

[30] Horowitz, S.L. and Pavlidis, T. Picture segmentation by a tree traversal algorithm. *Journal of the ACM*, 23(2):368-388 (1976).